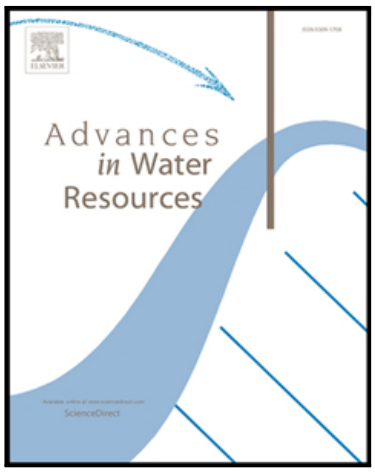

Fast laboratory-based micro-computed tomography for pore-scale research: illustrative experiments and perspectives on the future

Tom Bultreys , Marijn A. Boone , Matthieu N. Boone , Thomas De Schryver , Bert Masschaele , Luc Van Hoorebeke , Veerle Cnudde

PII: S0309-1708(15)00106-2
DOI: 10.1016/j.advwatres.2015.05.012
Reference: ADWR 2384

To appear in: *Advances in Water Resources*

Received date: 19 March 2015
Revised date: 12 May 2015
Accepted date: 13 May 2015

Please cite this article as: Tom Bultreys , Marijn A. Boone , Matthieu N. Boone , Thomas De Schryver , Bert Masschaele , Luc Van Hoorebeke , Veerle Cnudde , Fast laboratory-based micro-computed tomography for pore-scale research: illustrative experiments and perspectives on the future, *Advances in Water Resources* (2015), doi: 10.1016/j.advwatres.2015.05.012

Highlights

- State of the art in fast laboratory-based X-ray micro-computed tomography is outlined
- Real-time, pore-scale visualization of drainage in Bentheimer with lab-based scanner
- Solute transport is imaged at the pore scale in a limestone at 12 seconds per scan

Fast laboratory-based micro-computed tomography for pore-scale research: illustrative experiments and perspectives on the future

Tom Bultreys[a], Marijn A. Boone[a,b], Matthieu N. Boone[c], Thomas De Schryver[c], Bert Masschaele[b,c], Luc Van Hoorebeke[c] and Veerle Cnudde[a]

[a]UGCT/PProGRess, Dept. of Geology and Soil Science, Ghent University, Krijgslaan 281 (S8), 9000, Ghent, Belgium

[b]X-Ray Engineering bvba, De Pintelaan 111, 9000 Ghent, Belgium

[c]UGCT/Radiation Physics, Dept. of physics and astronomy, Ghent University, Proeftuinstraat 86, 9000 Ghent, Belgium

Corresponding author:

Tom Bultreys
Dept. of Geology and Soil Science/Centre for X-ray Tomography (UGCT), Ghent University
Krijgslaan 281 (S8)
9000 Ghent
Belgium
Tom.Bultreys@UGent.be
Tel: +32(0)9 264 46 33

Key points

-The current state of the art in fast (sub-minute) laboratory-based X-ray micro-computed tomography is outlined

-Drainage in Bentheimer is visualized in real time at the pore scale with a laboratory-based scanner

-Solute transport of a tracer salt is imaged at the pore scale in a limestone sample at 12 seconds per scan

Abstract.

Over the past decade, the wide-spread implementation of laboratory-based X-ray micro-computed tomography (micro-CT) scanners has revolutionized both the experimental and numerical research on pore-scale transport in geological materials. The availability of these scanners has opened up the possibility to image a rock's pore space in 3D almost routinely to many researchers. While challenges do persist in this field, we treat the next frontier in laboratory-based micro-CT scanning: in-situ, time-resolved imaging of dynamic processes. Extremely fast (even sub-second) micro-CT imaging has become possible at synchrotron facilities over the last few years, however, the restricted accessibility of synchrotrons limits the amount of experiments which can be performed. The much smaller X-ray flux in laboratory-based systems bounds the time resolution which can be attained at these facilities. Nevertheless, progress is being made to improve the quality of measurements performed on the sub-minute time scale. We illustrate this by presenting cutting-edge pore scale experiments visualizing two-phase flow and solute transport in real-time with a lab-based environmental micro-CT set-up. To outline the current state of this young field and its relevance to pore-scale transport research, we critically examine its current bottlenecks and their possible solutions, both on the hardware and the software level. Further developments in laboratory-based, time-resolved imaging could prove greatly beneficial to our understanding of transport behavior in geological materials and to the improvement of pore-scale modeling by providing valuable validation.

Keywords

4D micro-computed tomography, dynamic imaging, pore scale, drainage, solute transport

Manuscript

1 GENERAL INTRODUCTION

Understanding how fluids migrate through porous rocks and how this affects the minerals inside that rock is essential in numerous geological applications, going from the formation and weathering of geological materials (e.g. building stones) to the production and storage of fluids in geological reservoirs. Although fluid migration influences the behavior of these geological materials on the macroscopic scale (meter to kilometer scale for building stones and geological reservoirs, respectively), the essential flow and alteration processes occur on the pore scale (nanometer to micrometer scale), between the minerals of the porous geological material. Comprehending the underlying pore scale processes is crucial to make accurate predictions and decisions regarding important challenges like CO_2-sequestration, environmental remediation of polluted aquifers, enhanced oil recovery and cultural heritage preservation. Of particular interest in this regard are multi-phase and multi-component (reactive) fluid flow, and the coupling of mechanical deformation or failure of the material of interest with such flow phenomena.

Understanding the pore scale behavior which controls these processes, however, is a difficult problem which requires three-dimensional pore space characterization. Pore spaces in geological materials often have a complex microstructure, which can span the centimeter to the nanometer scale and can be very heterogeneous in nature. Therefore, their characterization requires more than experiments which measure global information like porosity and pore size distribution. Three-dimensional imaging techniques fill this requirement by providing local geometrical and topological information. The most mature experimental technique in this category is X-ray micro-computed tomography (micro-CT) [1,2]. Before, researchers either had to extrapolate two-dimensional measurements to obtain pseudo-three-dimensional volume information or perform laborious serial sectioning experiments to obtain such local information. Micro-CT however allows the non-destructive visualization of internal pore space structures in three dimensions. The recent increase in the availability of laboratory-scale micro-CT instrumentation has enabled many researchers to characterize the pore space of geomaterials in 3D on an almost routine basis, although a number of limitations in both the acquisition and the analysis of micro-CT data persist. For example, the attainable spatial resolution is often on the order of 1 to a few microns and depends on the size of the studied sample, while the acquisition time is typically on the order of 30 minutes to a few hours.

While 3D pore space characterization is an essential part of any pore scale transport or degradation study, it does not provide insight into the dynamics of the processes under investigation. To avoid image blurring (and other motion artifacts), the imaged sample should remain unchanged during the micro-CT acquisition. Therefore, there is a need for fast, time-resolved 3D (i.e. 4D) imaging of a material's microstructure while such a process is taking place, as the only alternative is imposing quasi-static conditions by halting the process during every imaging experiment [3]. Extremely fast micro-CT imaging has become available at synchrotrons over the last few years, attaining even a sub-second time resolution [2–5]. Although a comprehensive review of dynamic experiments performed at synchrotrons is out of the scope of this article, we mention some notable examples of pore scale imaging (in a geological context) at the sub-minute time scale of two-phase flow [6–9] and reactive flow [10]. Other examples of fast imaging of porous media at synchrotron institutions can be found in [11–13]. While synchrotron experiments are proving very valuable, the restricted accessibility of synchrotrons limits the amount of experiments which can be performed. Therefore, the development of laboratory-based fast (sub-minute) micro-CT scanning can prove important, as it would drastically increase the availability of 4D imaging with sub-minute time resolutions. Fast lab-based micro-CT would also allow researchers to prepare 4D experiments in the lab

before performing them with higher temporal or spatial resolutions and with better image quality at a synchrotron. This would be of high value to help optimize the use of synchrotron beam time.

Despite the desirability of fast lab-based micro-CT, the much smaller X-ray flux in lab-based systems bounds the time resolution which can be attained. Just like an underexposed photograph appears noisy due to photon counting statistics, the restriction on the X-ray flux in laboratory sources limits the image quality for short acquisition times. Other complications which may occur are for example insufficient angular sampling, too long detector read-out times and limited rotation speed. Despite the fact that rather little attention has been given to this topic in the literature (with the exception of work performed by researchers at the Australian National University [14–16]), advances in micro-CT hardware and in reconstruction and analysis software are starting to render sub-minute pore-scale experiments possible at laboratory set-ups. In this work, we illustrate this by the visualization of drainage of a Bentheimer sandstone and convective/diffusive mass transport of a salt (CsCl) in a water-saturated Savonnières limestone. In both experiments, the acquisition time per full micro-CT scan was 12 seconds, with a voxel size of 14.8 µm. While, naturally, the data quality is not as good as what can be expected from similar experiments performed at synchrotrons, we show that the obtained quality is sufficient to visualize many interesting aspects of the investigated transport processes in individual pores, even without applying special reconstruction algorithms. To our knowledge, the experiments reported in this work are the fastest in-situ, lab-based pore-scale micro-CT measurements of this kind described in the literature until now. Figure 1 illustrates the progress in attainable spatial and temporal resolution in micro-CT over the years, both at synchrotron and in typical laboratory-sources [3].

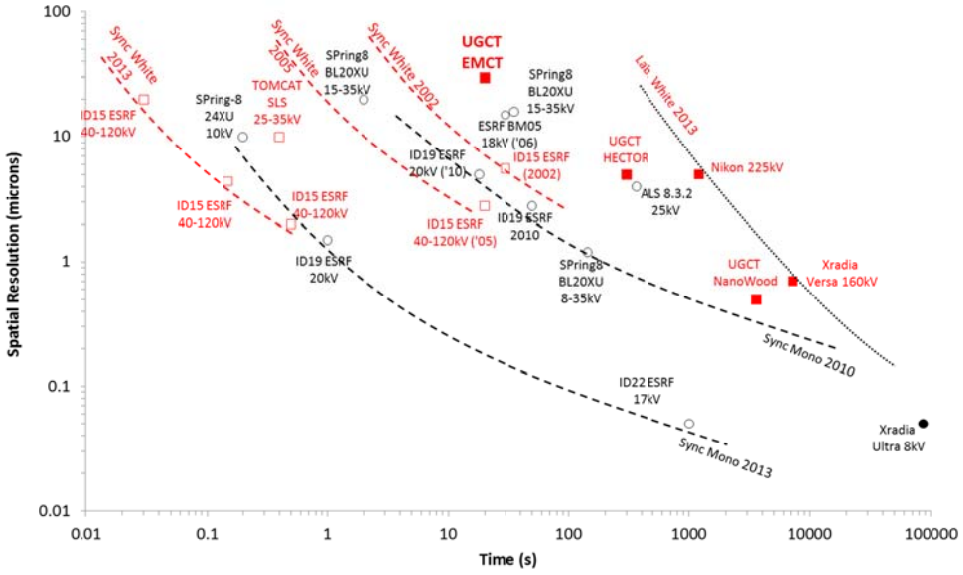

Figure 1. This figure (adapted from [3]) shows temporal and spatial resolutions attained at different synchrotron beamlines and lab set-ups. Open symbols denote synchrotron sources, while filled ones represent laboratory sources, squares denote polychromatic ("white") beam and circles denote monochromatic scanners. In cases where the spatial resolution is not cited, an estimated resolution of twice the voxel size is used. We follow this convention to report the spatial resolution in our own experiments. The reported time is the time needed to gather 1000 projections.

Given the importance of the development of fast 4D lab-based micro-CT to the pore scale modeling and experimentation community, we describe the current state of the art and the expected future development

of this field. Note, however, that this work is not intended as a comprehensive review but rather aims to provide a concise outline of the current and future possibilities of this experimental technique. In section 2, we discuss the optimization of various hardware and software components. In section 3.1, we show the real-time imaging of drainage at the pore scale in a Bentheimer sandstone, and in section 3.2 the imaging of advective-diffusive mass transport of a tracer salt in a water-saturated limestone is presented. These experiments simultaneously illustrate the use of fast 4D lab-based tomography in pore scale experiments and the current state of the art of this method.

2 TECHNOLOGICAL ADVANCES

In order to obtain a high-quality micro-CT scan, the accumulated X-ray dose in the detector during the acquisition of the projection images has to be sufficiently high, as the signal-to-noise ratio varies approximately as the square root of the amount of photons which hit the detector. In laboratory-based micro-CT systems, this sets a lower limit to the acquisition time, as the used X-ray flux emitted by the X-ray source is typically low (taking into account also the necessary minimum distance between the source and the detector, due to considerations regarding image magnification, sample size and cone beam artifacts). The limitations of these sources with respect to dynamic imaging are explained in section 2.1.1, as well as technological developments which might mitigate these limitations in the future. Other limitations on the image acquisition may be posed by the X-ray detector (section 2.1.2). During dynamic experiments on porous materials, the sample conditions are usually controlled in some way (e.g. applying mechanical loading, imposing (reactive) fluid flow, controlling temperature and humidity). Therefore, the sample usually has to be contained in a cell or a similar set-up. These cells can affect the image quality, and should therefore be designed carefully (section 2.1.3).

After treating the hardware challenges, we discuss the possibilities of smart image reconstruction and analysis to compensate for low image quality (section 2.2). Fast scans, acquired while dynamic processes are going on in the pore space, can and should be supplemented with as much prior information as possible. In many experiments, prior information about the pore geometry can be acquired with a long, high-quality scan while the sample is in static conditions. Other prior information might pertain to the dynamic process itself, for example, in immiscible two-phase flow experiments the assumptions of incompressible fluids and the presence of only three material phases can improve reconstructions with a limited number of projections [14]. By scanning faster, the quality will typically decrease, hence approaches using a priori information gain importance. Another principle which we expect will prove important in the future, is the incorporation of the time dimension in the image analysis. On the one hand, there is a need for software tools which allow researchers to track changes in their sample over time (e.g. deformation of a sample, velocities of fluid interfaces) and help them to make sense of the typically huge amount of data they acquire during a dynamic experiment. On the other hand, truly treating micro-CT time series data as 4D datasets may improve image analysis results, as it allows to incorporate more information. However, one thing is certain: 4D data analysis is computationally intensive, both when it comes to data storage as processing. Section 2.2.2 treats these challenges and opportunities.

2.1 HARDWARE EVOLUTIONS

2.1.1 X-ray Sources

X-ray sources in laboratory-based micro-CT set-ups are typically microfocus X-ray tubes, in which an electron beam is focused on a very small focal spot on the anode target. When the electrons hit the target after being accelerated by a high-voltage electric field, they create X-rays through their interaction with

the anode material. The main limitation of laboratory-based micro-CT in the scope of fast image acquisition is posed by the X-ray source. Unlike synchrotron sources, which exhibit very high brilliance, traditional laboratory sources have a limited X-ray output due to the power dissipation limitation when the electrons hit the anode target, implying longer acquisition times. Indeed, the energy efficiency of X-ray production in the form of Bremsstrahlung in this set-up is only about 1%, and a large portion of electron beam energy is deposited as heat. The power density limit of approximately 2W/µm² in the target is close to the fundamental limit at which material vaporization starts taking place, despite efforts of rotating anode systems [2]. As a result, the maximum achievable X-ray flux in laboratory systems is strongly correlated with the achieved focal spot size, and hence inversely correlated to the achievable image resolution. This resolution is important to resolve a pore space with sufficient detail (typical geological pore-scale micro-CT studies employ resolutions of 1^3 to 20^3 µm³ with acquisition times increasing strongly for higher resolutions, see Figure 1).

Recently, the invention of the liquid metal-jet X-ray source has mitigated the power density limit in laboratory X-ray sources. In this set-up, the anode target is a thin jet of liquid metal, hence renewing the target material constantly to avoid vaporization. The liquid metal-jet tubes are commonly used for X-ray diffraction (e.g. [17,18]), but have also proven their value for high-resolution X-ray imaging [19–22]. For the imaging of pore-scale dynamics, their applicability can be limited by the lower limit of the focal spot size (approximately 5-6 µm) and the low energy of the generated X-rays, caused by the low atomic numbers of the materials used as liquid metal. Recently, a setup using Indium (characteristic Kα energy 24.2 keV) has also been used for hard X-ray imaging [23,24]. When spatial resolutions better than 5-6 µm (hence smaller focal spot sizes) are required, transmission-type X-ray tubes need to be used. Nowadays, several manufacturers offer transmission targets on diamond substrate, allowing for an improved heat dissipation as compared to conventional beryllium substrates. Nevertheless, the highest achievable output power is relatively low due to the absence of direct, active cooling of the target.

Other alternative X-ray sources are based on inverse Compton-scattering [25,26]. While such sources may become more accessible in the future, they are not treated here in detail as they are currently still under development and not yet commercially available on a large scale.

2.1.2 X-Ray Detectors

Due to the limited X-ray flux achievable with conventional laboratory-based sources, image acquisition should be as efficient as possible. In laboratory conditions, this usually means that large flat-panel detectors with thick scintillators need to be used. In recent years, the highest achievable frame rate of these systems has drastically increased to values ranging from several tens of frames per second for full-frame acquisition to several hundreds of frames per second for limited region readout, while several experimental detector systems perform even better [27,28]. At the same time, the increased availability of large amounts of fast computer memory allowed for the implementation of fast acquisition schemes, no longer limited by the processing speed of hard drives. These two developments have drastically increased the possibilities of fast and continuous CT scanning. When even higher scanning rates are needed, high-speed line detector systems are to be used. However, they can scan only one or several lines at a time, drastically limiting the field-of-view and therefore the ability of these setups to create 3D images. For both detector types however, the temporal behavior of scintillators may in some cases become an issue at high frame rates (i.e. cause detector lag).

As an alternative to flat-panel detectors with scintillators, direct or hybrid detector systems have been developed over the last few years. These detector systems have no scintillator screen, but convert the absorbed X-rays directly into electron-hole pairs. This detection method increases the response speed, and allows for energy discriminating possibilities based on pulse height analysis. The latter allows for energy-

dispersive acquisition and for a drastic reduction of electronic noise. These systems have been reported to have frame rates in the kHz range [29,30]. These very high frame rate detectors are primarily developed for synchrotron applications [31,32] such as ptychographic imaging [33]. Consequently, they often use Si as detecting material, given the low X-ray energy typically used in coherent diffractive imaging. Using materials such as CdTe, which have a larger efficiency at high X-ray energies [34], the further developments of photon counting detectors may in the near future also benefit laboratory-based dynamic CT scanning.

2.1.3 Add-on equipment for sample conditioning

To investigate how fluids migrate through pores in a rock or how the minerals in the rock react over time, the geological sample needs to be subjected to controlled external conditions, e.g. mechanical loading [35], temperature [36] or humidity, possibly combined with the injection of pressurized liquids or gasses [37]. Specialized add-on equipment for the micro-CT setup is thus needed in order to visualize the sample at the desired in-situ conditions. It is not the intended scope of this paper to give a comprehensive overview of add-on equipment used for in-situ imaging applied in the literature, but rather to briefly highlight the limitations and challenges brought forth by this equipment, more specifically by flow cells. The main concerns related to such flow cell setups, especially for fast laboratory-based micro-CT imaging, are the size of the setup and the materials out of which it is constructed. Lab-based micro-CT commonly achieves geometrical magnification by using conical X-ray beams. This means that the diameter of the flow cell should be small in order to achieve high magnifications and correspondingly high resolutions (depending on the characteristics of the scanner) while simultaneously maximizing the use of the available X-ray flux (i.e. without having to increase the focus-detector distance more than necessary) [1,16]. This is crucial to discriminate the pore network in the sample with sufficient detail. Furthermore, the parts of the cell which are in the field of view should attenuate the X-ray beam as little as possible to maximize the X-ray flux. At low cell pressures, low-cost plastics (e.g. PMMA) and epoxies [38,39] are suitable, as these have a low X-ray attenuation coefficient compared to most geological materials. However, to simulate reservoir conditions, high pressures (typically 100 - 500 bar) and temperatures (typically 50-200°C) are required. The steel alloys (e.g. hastelloy) which are typically used to build Hassler cells for flow experiments at these conditions are highly attenuating and therefore not suitable for X-ray micro-CT imaging. Instead, imaging experiments require miniature Hassler cells constructed out of weakly attenuating, strong materials like aluminum [40], carbon-based materials [41–43], beryllium [2], and special plastics like PEEK [37].

2.2 SOFTWARE ADVANCES

2.2.1 Advances in reconstruction algorithms

In addition to specific requirements for acquisition hardware to optimize 4D scanning, major improvements can also be achieved by applying clever software algorithms, mainly in terms of tomographic reconstruction. The main challenge posed by laboratory-based fast CT is Poisson noise, induced by the limited X-ray flux. Additionally, structural changes of the scanned sample during a CT acquisition will cause motion blurring artefacts which deteriorate the reconstruction quality. Methods to cope with both motion blurring and bad image statistics are thus crucial in dealing with fast imaging of dynamic processes.

Currently, most tomographic reconstructions are performed using analytical filtered back-projection (FBP) methods, such as the Feldmann-Davis-Kress (FDK) algorithm [44,45]. These algorithms have the advantage of being relatively simple and fast in terms of computational complexity, but theoretically they are only valid in idealized cases (i.e. when enough projections are acquired). In the context of (dynamic)

CT imaging, iterative reconstruction techniques [46,47] have gained much interest. During iterative reconstruction, intermediate solutions of the reconstructed 3D object are incrementally refined by simulating projection images from this solution (by forward projection) and subsequently adapting it to better reproduce the experimental projections. Unlike analytical algorithms, the iterative techniques can incorporate a priori knowledge about the measured object, drastically decreasing the degrees of freedom in the reconstruction process. Furthermore, accurate models for specific physical and geometrical features of the acquisition process can be modeled into the reconstruction, opening the possibility to include corrections for imaging artifacts, e.g. beam hardening [48,49].

In general, a priori knowledge in CT leverages the spatial and temporal correlations which exists between neighboring voxels in a volume throughout time. It can be implemented in several ways, e.g. by assuming the scanned object is only made up of a limited number of clearly separated materials, corresponding to an equally limited number of discrete gray values. This is typically done by a segmentation of the intermediate result before a forward projection is performed. In doing so, the final result can typically be obtained using fewer projection images, and no longer contains image noise. Furthermore, as image segmentation is in most cases the first step in 3D analysis, these reconstruction methods have the capability to make this processing step obsolete. Several reconstruction algorithms for this so-called *discrete tomography* have been developed in recent years [50–52]. They differ mainly in the segmentation method, in the moment of the appearance of the segmentation in the flow of the algorithm, and in additional strategies to reduce noise effects in the segmentation of (partially) reconstructed volumes.

Another way of using prior knowledge is to incorporate information about the object's shape. The simplest approach is to provide an appropriate initial intermediate solution to the iterative reconstruction method. The drawback of this method is that this initial solution can become too dominant, obscuring details which are actually changing in time. Other, more advanced methods indirectly incorporate the initial solution by reconstructing the difference between the initial volume and the temporally changing volume, as in prior image constrained compressed sensing (PICCS) [53,54]. Indeed, the difference between these volumes will primarily highlight the regions of the volume which are structurally changing through time. One of the more accomplished iterative reconstruction method for dynamic porous media applications so far has been developed at ANU, and combines the notion of compressed sensing (cfr. PICCS) with discrete tomography [15,55,56]. The method has been used for two-phase flow experiments and formulates the reconstruction as an optimization problem over all discrete two-grey level solutions which honor the static pore structure, while accommodating for the expected physical two-phase flow behavior by adding extra regularization terms to the optimization cost function.

The dynamically evolving regions can also be estimated directly from the dynamic CT data itself, i.e. without introducing an initial solution [57]. Finally, temporal correlations can be exploited by modeling the expected deformation of the object as a function of time [58]. However, computational feasibility limits the number of parameters, which restricts the deformation models to fairly global ones, affecting the object as a whole, e.g. affine deformations.

It should be clear that aforementioned methods are only valid within specific constraints. Discrete reconstruction methods are not applicable for complex multi-material objects where partial volume effects are important. They are however very well suited for the imaging of homogeneous structures which are changing in time, e.g. foams under compression. Methods applying initial solutions on the other hand are well suited for the imaging of rigid structures in which small regions are changing in time, e.g. fluid flow through a geological sample. Vast, non-local, structural changes however are more difficult to correct for with these methods, in this case the reconstruction methods based on deformation models are more suitable.

Next to alterations in the reconstruction step, some methods also rely on image pre-processing, by altering the projection. This is quite often the case for noise reduction methods or phase retrieval algorithms, some of which inherently include noise reduction. In filtered back-projection methods, the filter may also be adapted in order to reduce noise (typically at the expense of image sharpness).

2.2.2 4D image analysis

As the signal-to-noise ratio is of major concern in lab-based fast micro-CT, it may prove very important to make use of the redundancy of information in the time sequence when analyzing the data. This way, it should be possible to improve the 3D analysis (e.g. [2,59–61]) at one fixed time point by incorporating information from other time points. For example, 4D filtering methods may be useful to reduce motion artifacts and even to compensate for noisy data. To our knowledge, very little work on this topic has been done in the context of high-resolution CT research. However, we see a large potential for methods which have recently been developed for medical imaging purposes, e.g. 4D filters designed for CT perfusion scans [62–64] and for magnetic resonance imaging [65,66].

Another key principle to improve the quality of the analysis is the use of high quality scans performed at initial or final states of the sample. For example, one can segment the pore space from a prior high quality scan and use it as an analysis mask for the dynamic scans (as demonstrated in section 3 of this work). This rather simple approach is only applicable when the pore structure does not deform during the experiment and when the high-quality dataset can be spatially matched to the dynamic datasets (either by not moving the sample between acquisitions or by applying image registration algorithms, e.g. [67,68]).

Next to using redundant and prior information, 4D datasets call for algorithms to quantify a sample's evolution through time. In some cases it may be sufficient to perform 3D analysis on datasets of consecutive time steps and compare the results. It should be noted that in this case, it should be possible to script the process which may cause problems when user-defined input parameters need to be varied for each time step. In many cases, it is interesting to quantify changes through time by tracking movement or deformation of structures in the sample. Methods to do this are often inspired by 2D digital image correlation, and referred to as digital volume correlation. However, this problem is not specific to laboratory-based micro-CT as it is of interest in synchrotron-based and medical CT as well. For this reason, it is not treated here and the interested reader is referred to [3,69–75].

3 ILLUSTRATIVE APPLICATIONS

3.1 TWO-PHASE FLOW

The flow of multiple fluid phases in porous rocks is essential to several important geo-engineering challenges, e.g. environmental remediation of aquifers polluted with non-aqueous phase liquids (NAPL), hydrocarbon recovery and CO_2-sequestration in geological reservoirs. The field-scale properties of these processes are critically determined by pore-scale fluid-fluid and fluid-solid interactions. In this section, we present an experiment where drainage of a Bentheimer sandstone was visualized under dynamic conditions (i.e. while continuously injecting non-wetting fluid) on a laboratory-based micro-CT scanner at Ghent University's Centre for X-ray Tomography (UGCT). We show the observation of pore filling events which bear strong resemblance to Haines jumps, even though we did not record pressure measurements at the time of the experiment to prove this. To our knowledge, it is the first time observations of this kind have been made on a laboratory-based micro-CT system.

While a detailed explanation of the physics of drainage is out of the scope of this article, we outline the motivation to perform this experiment. During drainage, the displacement process happens by fast,

irreversible events (Haines jumps) alternated by smooth, reversible displacement related to fluid storage in pinned interfaces [76,77]. Such a Haines jump corresponds to the filling of a single geometrical pore body. These jumps frequently happen in cascades, classically explained as successive filling of pores with lower entry capillary pressure than the first pore of the cascade. The rate of non-wetting fluid injection does not influence the duration of individual Haines jumps, but it does influence their frequency. Single pore events have been found to transpire on the millisecond time scale [76], and [77] states that cascades of pore filling events take place on a time scale of typically 0.5 to 2 seconds. Clearly, to investigate dynamic effects related to the irreversible displacement, it is crucial not to interrupt the non-wetting fluid injection during the imaging. In their groundbreaking work on real-time visualization of two-phase flow in natural stone, executed at the TOMCAT beamline of the Swiss Light Source synchrotron facility, Berg et al. [6] were able to perform such an experiment for the first time. In this study, they suggest that dynamic effects cause pore filling events to be non-local. Since then, this topic has been investigated further [77,78], yet many aspects of the occurring dynamic effects and particularly of their influence on larger-scale petrophysical properties remain unclear. Further imaging experiments may thus prove extremely valuable in understanding these processes.

3.1.1 Materials and methods

In this experiment, the sample was a German Bentheimer sandstone of the Gildehaus variety from the Early-Cretaceous. Its rather homogeneous pore size distribution render it ideally suited for micro-CT studies. A sample with a diameter of 6 mm and a height of 17 mm was put in a Viton sleeve and set into a custom-built, low-cost PMMA flow cell (Figure 2). The flowcell was mounted on UGCT's Environmental Micro-CT scanner (EMCT, Figure 2), designed and built in-house in collaboration with X-Ray Engineering bvba (XRE, Ghent, Belgium). This scanner is specially developed to image samples under controlled environmental conditions or during dynamic experiments. To allow for the sample and the equipment connected to it with wires or tubing to remain static, the setup has a rotating X-ray source and detector assembly on a gantry. This eliminates problems with flow instabilities caused by bending or twisting of the flow lines, and it helps avoid unwanted sample movement during the acquisition. Unlimited continuous rotation is possible because electrical power and safety interlocks are transmitted through slip-rings. The system is equipped with a standard directional microfocus X-ray tube with integrated high-voltage power supply (maximum high voltage 130 kV, maximum power output 39 W, minimum spot size 5µm). The detector is a CMOS flat-panel detector (1316 by 1312 pixels with a 100 µm pitch) with a thick, structured CsI scintillator. The GigE-interface permits frame rates of 30 fps at full resolution and 60 fps in 2x2 binned mode (and even more in panoramic mode). The scanner's source-detector combination, together with the applied smooth-scanning (rather than step-and-shoot) acquisition, allows for fast scanning. More details on EMCT's setup can be found in [79], although the rotation motor has since been upgraded to allow for faster scanning.

Figure 2. A custom-built PMMA confining-pressure flowcell (left) allows the visualization of fluid flow in stone samples with a diameter of 6 mm and a height between 15 and 20 mm. UGCT's EMCT scanner (right) was built in collaboration with XRE. The flow cell is mounted on a stand which moves into the scanner from below. The gantry (with the source and detector mounted on it) rotates around the sample, while the sample remains static.

The sample was first saturated with water by flushing with CO_2 and subsequently with water. At this point, a first high-quality scan (Table 1) of the sample was performed to obtain geometric information of the sample's pore space. Then, a highly X-ray-attenuating brine (10 wt% CsCl) was pumped through the sample. A second high-quality scan confirmed that the sample was completely brine-saturated. Subsequently, drainage was started by pumping an oil phase (kerosene or 'paraffin') into the sample at a flow rate of 6 µl/min. This corresponds to a capillary number [80] of approximately $7 \cdot 10^{-8}$, a realistic value for real reservoir flow processes. Fast scans were performed with settings outlined in Table 1. Projections were continuously acquired during a 5 minute time interval, during which the drainage was not halted (except near the beginning and end of the acquisition).

The fast scans were recorded and processed with the proprietary 4D tools of the ACQUILA software (XRE, Ghent, Belgium). Because the acquisition is continuous, projections acquired during any full rotation of the gantry can be reconstructed regardless of the starting angle. In this experiment, we generated a new reconstruction after every 120° rotation of the gantry, meaning consecutive reconstructions in the time series are 4 seconds apart. This results in a total of 72 reconstructions in the 5 minute acquisition. Tomographic reconstruction was performed with the FDK algoritm, implemented on the GPU.

Table 1. Settings of scans performed in the drainage experiments

	High quality	Fast scans
Voxel size (µm)	7.4	14.8
Total time per scan	21 min	12 s
Binning of detector pixels	No	Yes (2x2)
Amount of voxels/scan	1314x1314x1311	657x657x656
Projection exposure time (ms)	550	20
Projections per 360° scan	2200	600
Accelerating voltage (kV)	80	130
X-ray source output (W)	8	16
Source-detector distance (mm)	365.0	
Source-object distance (mm)	27.1	

3.1.2 Results and discussion

The high-quality scan of the pore space (filled with pure water) was segmented to identify pore and solid voxels. The fast scans were first treated with an anisotropic diffusion filter in Avizo (VSG/FEI, France) and then resampled without interpolation with a factor two to contain as many voxels as the high-quality scan. The oil phase was subsequently segmented from each fast scan, with the pore space identified from the high-quality scan applied as a mask. This way, prior information on the pore space geometry was incorporated post-reconstruction. This information can also be used during reconstruction, if some assumptions on the transpiring pore-scale process are made [14]. Using this approach, Myers and coworkers [14,15] reported lab-based scans of two-phase flow under dynamic conditions, at 85 seconds per scan with a voxel size of 12 µm.

After recombining the oil segmentations with the pore space segmentation, 3-phase segmentations (oil, water and solid) were obtained for each timestep. Example slices showing the segmentation quality can be seen in Figure 3 (additionally, example slices can be found in supplementary materials). While it is clear that the resolution of the scans is insufficient to detect the oil-phase in some of the smallest pores, the fast scans evidently contain much information on the rock's drainage behavior and allow pore filling events like the one circled in Figure 4 to be investigated. By comparison with results shown in [6], this figure is likely to show an individual Haines jump (note that the apparently gradual filling of the pore is due to remaining motion artifacts in the reconstruction). Further analysis of the experiment is presented in [81]. It can be concluded that it is becoming possible to visualize the fundamental pore-scale processes which govern drainage in geological porous media with laboratory-based micro-CT scanners, despite remaining challenges related to spatial and time resolution. With regard to the former challenge, it should be noted that the rather simple flow cell used in this work could be designed more efficiently. This way, it may be possible to minimize X-ray absorption by the cell and to reduce the source-to-sample distance, resulting in larger magnifications. With regard to the latter, selecting a set of projections representing a 360° rotation can be done more efficiently by detecting pore-scale events on the radiographs, in a similar way as shown by [8]. This method results in the elimination of motion artifacts for selected events.

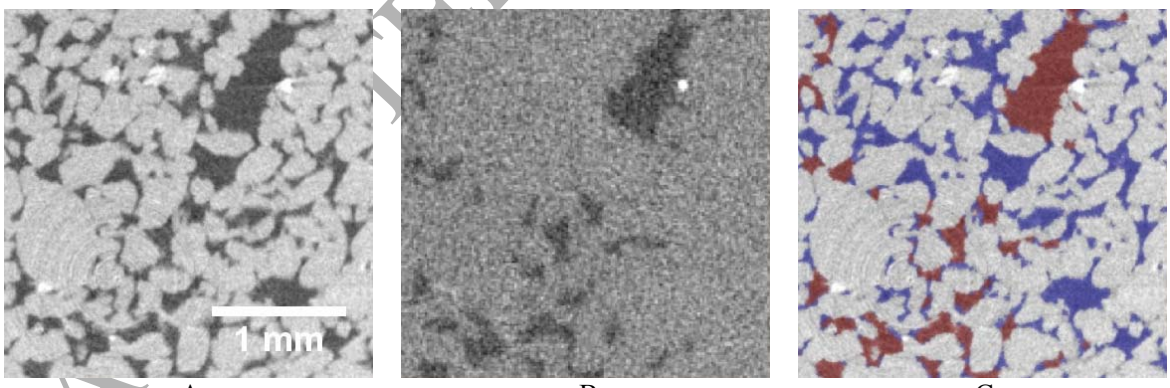

Figure 3. This figure suggests that the image quality is sufficient to visualize most oil-filled pores (with the exception of oil in very fine pore space features). Figure A shows a cropped slice from the high-quality scan (7.4 µm voxel size). By applying the pore space mask determined from A and segmenting the fast scan (12 s) in B, the pore space voxels were segmented into the oil phase (red) and the brine phase (blue) (C). Figure B was recorded after 4 minutes of running the drainage experiment (60th scan in the time series). Note that due to the highly-attenuating CsCl, the brine could not be distinguished from the stone in the fast scans.

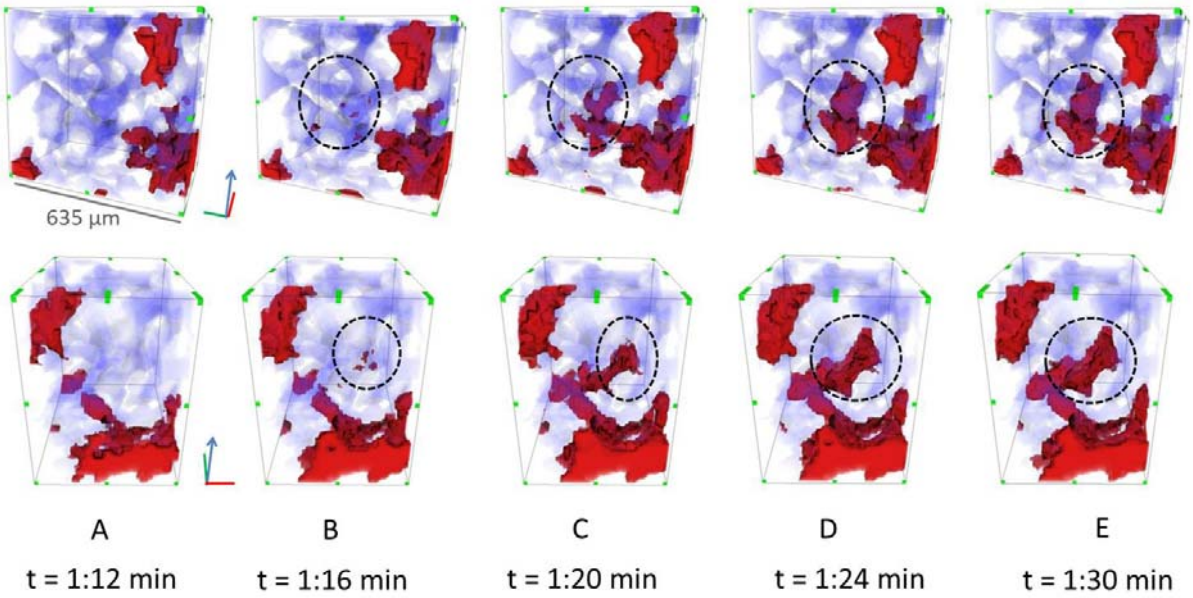

Figure 4. This time sequence shows a pore filling event (circled) during drainage from two viewing angles. The non-wetting phase is visualized in red, the wetting phase in transparent blue. The reported time is the starting time of the micro-CT acquisition. Each acquisition took 12 seconds.

3.2 SOLUTE TRANSPORT

In this section, we describe an experiment aimed at elucidating solute transport in heterogeneous rocks. In groundwater systems, mixing of reactants often limits (bio)chemical reactions [82]. In CO_2 sequestration and enhanced oil recovery, CO_2 dissolved in brine can trigger dissolution and precipitation of minerals in the host rock's pore space, in turn affecting this rock's mechanical and fluid flow properties [43]. The transport phenomena and simultaneous chemical reactions in these processes are coupled, and one can therefore only begin to understand the dissolution and precipitation patterns and the resulting flow properties, if one also understands solute transport by advection and diffusion in the pore space. In heterogeneous media, particularly carbonates, the pore-level flow field can show significant channeling [83]. This implies that important differences in fluid chemistry can arise between the more stagnant regions and the channels with a higher advective transport rate, which in turn will influence the dissolution behavior in the carbonate host rock. Depending on the balance between advection, diffusion and reaction rates, the dissolution reaction can cause the preferential flow channels to become increasingly wide. This behavior is often referred to as wormholing [84], and can have important field-scale consequences (e.g. [85]).

We show the feasibility of imaging solute transport (diffusion and advection) in 3D in a carbonate at the pore scale. While some studies have investigated the imaging of solute transport [86–89] , to our knowledge this has not been undertaken before simultaneously at the pore scale and at the time scale (12 seconds per scan) shown here. While the discussion will be restricted to one experiment (a single imposed flow rate), by varying the flow rate a detailed study of pore scale dispersion can be undertaken. Such studies may prove vital as a validation to solute transport modeling methods described in for example [90,91] and as input to characterize the connectivity of microporosity in multi-scale modeling [92,93].

3.2.1 Materials and methods

In the experiment outlined here, transport of a tracer salt subject to diffusion and advection is investigated in the Savonnières limestone, a French oolithic limestone (Late Jurassic). This grain-supported limestone consists of ooids and shell fragments bound together by sparite. During diagenesis, some of these grain fragments were partially dissolved resulting in a pore network with well-connected pores between the grains (intergranular porosity) and secondary porosity inside the dissolved grains (intragranular porosity or vuggy porosity), which is connected to the rest of the pore network through microporosity [94]. Preferential flow channels were visualized by pumping a highly X-ray attenuating brine (containing 10 wt% CsCl) into a water-saturated sample at a flow rate of 0.6 ml/min. The sample had a diameter of 6 mm and was placed in the PMMA flow cell (Figure 2). Fast laboratory-based micro-CT scans were performed with EMCT (12 seconds/scan). Scan parameters were the same as the fast scans described in section 3.1.1. Similarly to the workflow described in that section, a high-quality scan was used to segment a mask for the macropores.

3.2.2 Results and discussion

In Figure 5, the histogram of the reconstructed image intensity values inside the macropore voxels (selected by applying the pore space mask) in the limestone is given for the different timesteps. The peak at 0 seconds shows the distribution of the intensity values before brine injection. At this stage, all voxels included in the histogram (i.e. all voxels in the macro-pore space) are filled with pure water. This is also illustrated in the rendering in this figure, where at 0 seconds the image intensity values in the pore space are low and homogeneously distributed. During injection, the histogram shifts to the right and after 96 seconds, the intensity values are distributed in two peaks. This indicates a heterogeneous distribution of the CsCl concentration in the pore space of the limestone sample. The renderings show that most of the intergranular pore space contains a high CsCl concentration, while the intragranular pores in the dissolved ooids (Figure 5, dotted circle) still have a low CsCl concentration. In later timesteps, the peak on the left side of the histogram starts to disappear. This corresponds to the gradual increase of the CsCl concentration in the intragranular pores, which can be seen in the renderings. After a long waiting time, the histogram of the pore space voxels will again consist of one single peak, but centered around a higher average grey value than in the initial condition.

The results illustrate that the distribution of the brine in the intergranular pore space is mainly controlled by advection. In these pores, preferential flow paths can be found. The flow in the intragranular pores is more stagnant and the concentration of CsCl in this vuggy pore space is therefore mainly controlled by diffusion. Fitting with the scope of this article, more elaborate analysis of the data will be presented elsewhere. Although the measurements presented here are clearly a good indication of CsCl-concentrations in the sample, further research will be performed to calibrate the image intensity values to exact concentration values.

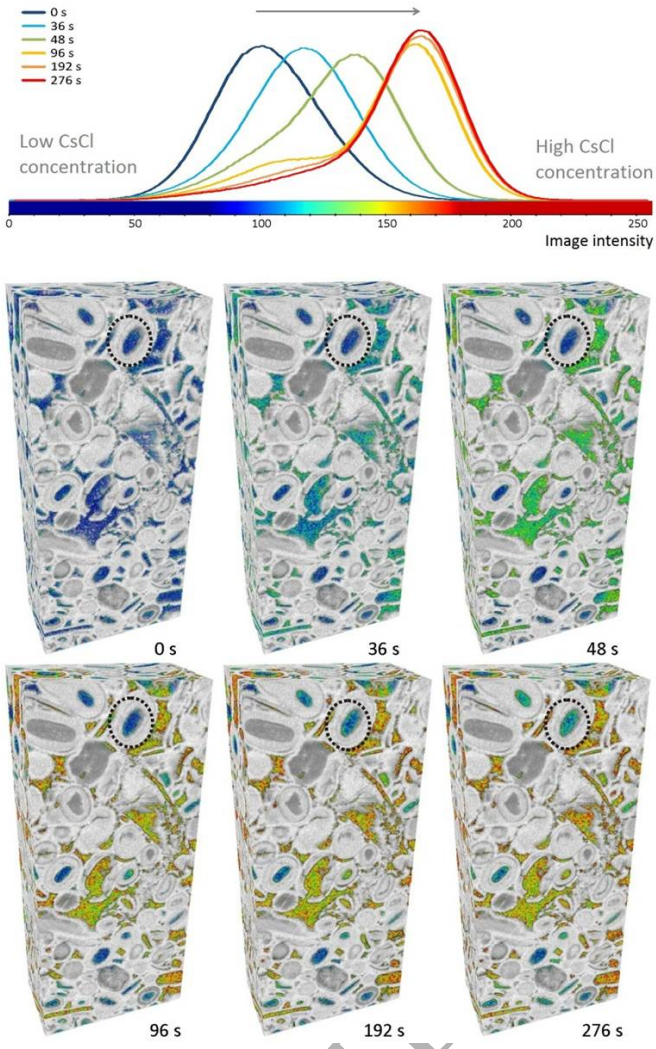

Figure 5. The graphs show the evolution of the image intensity histograms of (only) the pore space voxels in the Savonnières limestone sample during brine injection. High image intensities correspond to high CsCl-concentrations. The corresponding 3D rendering show the evolution of the CsCl concentration in the macropores. The dotted circle indicates an intragranular pore in which the flow is stagnant. Time series measurements were performed with the EMCT-scanner at an acquisition time of 12 seconds.

4 CONCLUSIONS

Micro-CT scanning with a sub-minute time resolution is a very desirable experimental technique, both as an accessible stand-alone tool to investigate dynamic pore-scale processes and to prepare experiments for much more restricted yet higher-quality synchrotron measurements. A number of difficulties, mainly related to the limited X-ray flux, have hampered the implementation of such set-ups. Future developments in X-ray source and detector technology (notably the improvement and implementation of liquid-metal jet sources and photon-counting detectors) may increase the attainable time resolution and improve the image quality and spatial resolution at short acquisition time. We also expect a significant contribution

from advanced tomographic iterative reconstruction and 4D image analysis algorithms, which can compensate for the often limited image quality in fast scans by incorporating prior information about the pore structure or the physical processes transpiring in the pore space. Furthermore, progress is being made in automating 4D image processing and image analysis, making it more and more feasible to work with large, computationally intensive time-series datasets.

Despite the limitations, we illustrate the large potential of fast micro-CT scanning with two cutting-edge real-time imaging experiments. We show that it is possible to visualize single and few-pore drainage events in a Bentheimer sandstone by continuously scanning the sample with UGCT's Environmental Micro-CT (EMCT) scanner at an acquisition time of 12 seconds per full rotation. The same set-up and settings were used to visualize pore scale solute transport of a tracer salt (CsCl) in a Savonnières limestone, allowing to study the location of stagnant and fast flow regions and the relative time scales of diffusion and advection in this stone.

As illustrated by these experiments, it is today becoming possible to study transport processes in geological samples at the pore scale in a laboratory-setting, without having to impose quasi-static conditions. We expect that with further improvements in image quality, real-time imaging with laboratory-based micro-CT scanners will be implemented much more widely. This would provide valuable feed-back to the pore scale modeling community and has the potential to strongly increase our understanding of porous media behavior. In the long term, this may be beneficial to the management of geological reservoirs and aquifers, as well as to a wide variety of other issues involving porous materials (e.g. building stone deterioration, development of batteries and fuel cells, food engineering, textile engineering).

ACKNOWLEDGEMENTS

We thank Dr. Rémi Blanc (FEI) for his assistance with handling 4D datasets in Avizo. Ioannis Zarikos is acknowledged for helping to build and test the flow set-up (shown in section 3) during his master's thesis. Dr. Hannelore Derluyn is thanked for helpful discussions. The Agency for Promotion of Innovation by Science and Technology in Flanders, Belgium (IWT) is acknowledged for the PhD grant of Tom Bultreys. The UGent Special Research Fund (BOF) is acknowledged for the post-doctoral grant of M.N. Boone. This work was also partially supported by FWO, project G024212N and G.0041.15N.

BIBLIOGRAPHY

[1] Cnudde V, Boone MN. High-resolution X-ray computed tomography in geosciences: A review of the current technology and applications. Earth-Science Rev 2013;123:1–17. doi:http://dx.doi.org/10.1016/j.earscirev.2013.04.003.

[2] Wildenschild D, Sheppard AP. X-ray imaging and analysis techniques for quantifying pore-scale structure and processes in subsurface porous medium systems. Adv Water Resour 2013;51:217–46. doi:http://dx.doi.org/10.1016/j.advwatres.2012.07.018.

[3] Maire E, Withers PJ. Quantitative X-ray tomography. Int Mater Rev 2014;59:1–43. doi:10.1179/1743280413Y.0000000023.

[4] Mokso R, Marone F, Haberthür D, Schittny JC, Mikuljan G, Isenegger A, et al. Following Dynamic Processes by X-ray Tomographic Microscopy with Sub-second Temporal Resolution, 2011, p. 38–41. doi:10.1063/1.3625299.

[5] Rack A, Garcia-Moreno F, Schmitt C, Betz O, Cecilia A, Ershov A, et al. On the possibilities of hard X-ray imaging with high spatio-temporal resolution using polychromatic synchrotron radiation. J Xray Sci Technol 2010;18:429–41. doi:10.3233/XST-2010-0273.

[6] Berg S, Ott H, Klapp SA, Schwing A, Neiteler R, Brussee N, et al. Real-time 3D imaging of Haines jumps in porous media flow. Proc Natl Acad Sci 2013;110:3755–9. doi:10.1073/pnas.1221373110.

[7] Youssef S, Deschamps H, Dautriat J, Rosenberg E, Oughanem R, Maire E, et al. 4D Imaging of fluid flow dynamics in natural porous media with ultra-fast X-ray microtomography. Int. Symp. Soc. Core Anal., Napa Valley, USA: Society of Core Analysts; 2013.

[8] Armstrong RT, Georgiadis A, Ott H, Klemin D, Berg S. Critical capillary number: Desaturation studied with fast X-ray computed microtomography. Geophys Res Lett 2014;41:55–60. doi:10.1002/2013GL058075.

[9] Hoogland, F., P. Lehmann, F. Moebius, P. Vontobel DO. Liquid redistribution behind a drainage front in porous media imaged by neutron radiography. EGU Gen. Assem. Geophys. Res. Abstr., Vienna, Austria: EGU; 2013, p. EGU2013–8156.

[10] Menke H, Bijeljic B, Andrew M, Blunt MJ. Dynamic Pore-scale Imaging of Reactive Transport in Heterogeneous Carbonates at Reservoir Conditions. Energy Procedia 2014;63:5503–11. doi:10.1016/j.egypro.2014.11.583.

[11] Baker DR, Brun F, O'Shaughnessy C, Mancini L, Fife JL, Rivers M. A four-dimensional X-ray tomographic microscopy study of bubble growth in basaltic foam. Nat Commun 2012;3:1135. doi:10.1038/ncomms2134.

[12] Eller J, Roth J, Marone F, Stampanoni M, Wokaun A, Büchi FN. Towards Ultra-Fast X-ray Tomographic Microscopy of Liquid Water in PEFC. ECS Trans 2011;41:387–94. doi:10.1149/1.3635572.

[13] Sedighi Gilani M, Fife JL, Boone MN, Ghazi Wakili K. Dynamics of microcrack propagation in hardwood during heat treatment investigated by synchrotron-based X-ray tomographic microscopy. Wood Sci Technol 2013;47:889–96. doi:10.1007/s00226-013-0545-8.

[14] Myers GR, Kingston AM, Varslot TK, Turner ML, Sheppard AP. Dynamic tomography with a priori information. Appl Opt 2011;50:3685–90. doi:10.1364/AO.50.003685.

[15] GR Myers, AM Kingston, TK Varslot, ML Turner AS. Dynamic X-ray micro-tomography for real time imaging of drainage and imbibition processes at the pore scale. Int. Symp. Soc. Core Anal., Society of Core Analysts; 2011.

[16] Sheppard A, Latham S, Middleton J, Kingston A, Myers G, Varslot T, et al. Techniques in helical scanning, dynamic imaging and image segmentation for improved quantitative analysis with X-ray

micro-CT. Nucl Instruments Methods Phys Res Sect B Beam Interact with Mater Atoms 2014;324:49–56. doi:10.1016/j.nimb.2013.08.072.

[17] King A, Reischig P, Adrien J, Ludwig W. First laboratory X-ray diffraction contrast tomography for grain mapping of polycrystals. J Appl Crystallogr 2013;46:1734–40. doi:10.1107/S0021889813022553.

[18] Kaminski R, Nottingham G, Coppens P. An optical chopper for generation of short X-ray pulses to allow in-house time-resolved photocrystallography. J Appl Crystallogr 2014;47:1765–8. doi:10.1107/S160057671401961X.

[19] Larsson DH, Lundström U, Westermark UK, Arsenian Henriksson M, Burvall A, Hertz HM. First application of liquid-metal-jet sources for small-animal imaging: high-resolution CT and phase-contrast tumor demarcation. Med Phys 2013;40:021909. doi:10.1118/1.4788661.

[20] Zhou T, Lundström U, Thüring T. Comparison of two x-ray phase-contrast imaging methods with a microfocus source. Opt Express 2013;21:1141–8. doi:10.1364/OE.21.030183.

[21] Lundström U, Larsson DH, Burvall A, Scott L, Westermark UK, Wilhelm M, et al. angiography for sub-10 μm vessel imaging. Phys Med Biol 2012;57:7431–41. doi:10.1088/0031-9155/57/22/7431.

[22] Bartels M, Hernandez VH, Krenkel M, Moser T, Salditt T. Phase contrast tomography of the mouse cochlea at microfocus x-ray sources. Appl Phys Lett 2013;103. doi:10.1063/1.4818737.

[23] Espes E, Andersson T, Björnsson F, Gratorp C, Hansson BAM, Hemberg O, et al. Liquid-metal-jet x-ray tube technology and tomography applications. SPIE Opt. Eng. + Appl., International Society for Optics and Photonics; 2014, p. 92120J. doi:10.1117/12.2061612.

[24] Larsson DH, Takman PAC, Lundström U, Burvall A, Hertz HM. A 24 keV liquid-metal-jet x-ray source for biomedical applications. Rev Sci Instrum 2011;82. doi:10.1063/1.3664870.

[25] Eggl E, Schleede S, Bech M, Achterhold K, Loewen R, Ruth RD, et al. X-ray phase-contrast tomography with a compact laser-driven synchrotron source. Proc Natl Acad Sci 2015;112:201500938. doi:10.1073/pnas.1500938112.

[26] Graves WS, Bessuille J, Brown P, Carbajo S, Dolgashev V, Hong K-H, et al. Compact x-ray source based on burst-mode inverse Compton scattering at 100 kHz. Phys Rev Spec Top - Accel Beams 2014;17. doi:10.1103/PhysRevSTAB.17.120701.

[27] Krymski AI, Bock NE, Tu N, Van Blerkom D, Fossum ER. A high-speed, 240-frames/s, 4.1-Mpixel CMOS sensor. IEEE Trans Electron Devices 2003;50:130–5. doi:10.1109/TED.2002.806961.

[28] Singh B, Miller SR, Bhandari HB, Graceffa R, Irving TC, Nagarkar V V. High-speed detector for time-resolved diffraction studies. J Phys Conf Ser 2013;425. doi:10.1088/1742-6596/425/9/092005.

[29] Szczygiel R, Grybos P, Maj P. High frame rate measurements of semiconductor pixel detector readout IC. Nucl Instruments Methods Phys Res Sect A Accel Spectrometers, Detect Assoc Equip 2012;680:56–60. doi:10.1016/j.nima.2012.03.045.

[30] Dinapoli R, Bergamaschi A, Henrich B, Horisberger R, Johnson I, Kraft P, et al. A new family of pixel detectors for high frame rate X-ray applications. Nucl. Instruments Methods Phys. Res. Sect. A Accel. Spectrometers, Detect. Assoc. Equip., vol. 617, 2010, p. 384–6. doi:10.1016/j.nima.2009.10.043.

[31] Johnson I, Bergamaschi A, Billich H, Cartier S, Dinapoli R, Greiffenberg D, et al. Eiger: a single-photon counting x-ray detector. J Instrum 2014;9. doi:10.1088/1748-0221/9/05/C05032.

[32] Henrich B, Bergamaschi A, Broennimann C, Dinapoli R, Eikenberry EF, Johnson I, et al. PILATUS: A single photon counting pixel detector for X-ray applications. Nucl Instruments Methods Phys Res Sect A Accel Spectrometers, Detect Assoc Equip 2009;607:247–9. doi:10.1016/j.nima.2009.03.200.

[33] Guizar-Sicairos M, Johnson I, Diaz A, Holler M, Karvinen P, Stadler H-C, et al. High-throughput ptychography using eiger: scanning x-ray nano-imaging of extended regions. Opt Express 2014;22:14859–70.

[34] Koenig T, Schulze J, Zuber M, Rink K, Butzer J, Hamann E, et al. Imaging properties of small-pixel spectroscopic x-ray detectors based on cadmium telluride sensors. Phys Med Biol 2012;57:6743–59. doi:10.1088/0031-9155/57/21/6743.

[35] Bale H a, Haboub A, MacDowell A a, Nasiatka JR, Parkinson DY, Cox BN, et al. Real-time quantitative imaging of failure events in materials under load at temperatures above 1,600 °C. Nat Mater 2013;12:40–6. doi:10.1038/nmat3497.

[36] De Kock T, Boone M, Dewanckele J, Boever W De, Boone M, Schutter G De, et al. Monitoring frost susceptibility of limestone faces. 12th Int. Congr. Deterior. Conserv. Stone, vol. 1889, 2013.

[37] Boone MA, Nielsen P, De Kock T, Boone MN, Quaghebeur M, Cnudde V. Monitoring of stainless-steel slag carbonation using X-ray computed microtomography. Environ Sci Technol 2014;48:674–80. doi:10.1021/es402767q.

[38] Pak T, Butler I, van Dijke MIJ, Geiger S, Jiang Z. Visualisation of Two-Phase Fluid Displacement Processes at Pore Scale in Carbonate Rocks using Computed Tomography Technique. ICTMS2013, 2013, p. 5–8.

[39] Herring AL, Harper EJ, Andersson L, Sheppard A, Bay BK, Wildenschild D. Effect of fluid topology on residual nonwetting phase trapping: Implications for geologic CO2 sequestration. Adv Water Resour 2013;62:47–58. doi:10.1016/j.advwatres.2013.09.015.

[40] Fusseis F, Steeb H, Xiao X, Zhu W, Butler IB, Elphick S, et al. A low-cost X-ray-transparent experimental cell for synchrotron-based X-ray microtomography studies under geological reservoir conditions. J Synchrotron Radiat 2014;21:251–3. doi:10.1107/S1600577513026969.

[41] Iglauer S, Paluszny A, Pentland CH, Blunt MJ. Residual CO2 imaged with X-ray micro-tomography. Geophys Res Lett 2011;38:n/a – n/a. doi:10.1029/2011GL049680.

[42] Andrew M, Bijeljic B, Blunt MJ. Pore-scale imaging of trapped supercritical carbon dioxide in sandstones and carbonates. Int J Greenh Gas Control 2014;22:1–14. doi:10.1016/j.ijggc.2013.12.018.

[43] Ott H, de Kloe K, van Bakel M, Vos F, van Pelt A, Legerstee P, et al. Core-flood experiment for transport of reactive fluids in rocks. Rev Sci Instrum 2012;83:084501. doi:10.1063/1.4746997.

[44] Kak AC, Slaney M. Principles of computerized tomographic imaging. IEEE Press; 1988.

[45] Feldkamp L a., Davis LC, Kress JW. Practical cone-beam algorithm. J Opt Soc Am A 1984;1:612. doi:10.1364/JOSAA.1.000612.

[46] Herman GT, Lent A. Iterative reconstruction algorithms. Comput Biol Med 1976;6:273–94. doi:10.1016/0010-4825(76)90066-4.

[47] Andersen AH, Kak AC. Simultaneous algebraic reconstruction technique (SART): a superior implementation of the art algorithm. Ultrason Imaging 1984;6:81–94. doi:10.1016/0161-7346(84)90008-7.

[48] Brabant L, Pauwels E, Dierick M, Van Loo D, Boone MA, Van Hoorebeke L. A novel beam hardening correction method requiring no prior knowledge, incorporated in an iterative reconstruction algorithm. NDT E Int 2012;51:68–73. doi:10.1016/j.ndteint.2012.07.002.

[49] De Man B, Nuyts J, Dupont P, Marchal G, Suetens P. An iterative maximum-likelihood polychromatic algorithm for CT. IEEE Trans Med Imaging 2001;20:999–1008. doi:10.1109/42.959297.

[50] Brabant L, Dierick M, Pauwels E, Boone MN, Hoorebeke L Van. EDART, a discrete algebraic reconstructing technique for experimental data obtained with high resolution computed tomography. J Xray Sci Technol 2014;22:47–61. doi:10.3233/XST-130408.

[51] Herman GT, Kuba A. Advances in discrete tomography and its applications. Springer Science & Business Media. Springer Science & Business Media; 2008.

[52] Batenburg KJ, Sijbers J. DART: A Practical Reconstruction Algorithm for Discrete Tomography. IEEE Trans Image Process 2011;20:2542–53. doi:10.1109/TIP.2011.2131661.

[53] Chen G-H, Tang J, Leng S. Prior image constrained compressed sensing (PICCS): a method to accurately reconstruct dynamic CT images from highly undersampled projection data sets. Med Phys 2008;35:660–3. doi:10.1118/1.2836423.

[54] Lee J, Stayman JW, Otake Y, Schafer S, Zbijewski W, Khanna AJ, et al. Volume-of-change cone-beam CT for image-guided surgery. Phys Med Biol 2012;57:4969–89. doi:10.1088/0031-9155/57/15/4969.

[55] Myers GR, Kingston AM, Varslot TK, Turner ML, Sheppard AP. Dynamic tomography with a priori information. Appl Opt 2011;50:3685–90. doi:10.1364/AO.50.003685.

[56] Myers G, Varslot T, Kingston A, Herring A, Sheppard AP. Ground-truth verification of dynamic x-ray micro-tomography images of fluid displacement. vol. 8506, 2012, p. 85060P – 85060P – 7. doi:10.1117/12.929410.

[57] Van Eyndhoven G, Batenburg KJ, Sijbers J. Region-based iterative reconstruction of structurally changing objects in CT. IEEE Trans Image Process 2014;23:909–19. doi:10.1109/TIP.2013.2297024.

[58] Mooser R, Forsberg F, Hack E, Székely G, Sennhauser U. Estimation of affine transformations directly from tomographic projections in two and three dimensions. Mach Vis Appl 2013;24:419–34. doi:10.1007/s00138-011-0376-2.

[59] Kaestner a., Lehmann E, Stampanoni M. Imaging and image processing in porous media research. Adv Water Resour 2008;31:1174–87. doi:10.1016/j.advwatres.2008.01.022.

[60] Russ JC. The Image Processing Handbook. 4th ed. Boca Raton, FL: CRC Press; 2002.

[61] Brabant L, Vlassenbroeck J, De Witte Y, Cnudde V, Boone MN, Dewanckele J, et al. Three-dimensional analysis of high-resolution X-ray computed tomography data with Morpho+. Microsc Microanal 2011;17:252–63. doi:10.1017/S1431927610094389.

[62] Mendrik A, Vonken E -j., Witkamp T, Prokop M, van Ginneken B, Viergever M. Using the Fourth Dimension to Distinguish Between Structures for Anisotropic Diffusion Filtering in 4D CT Perfusion Scans. Spat. Image Anal. Longitud. Time-Series Image Data, Springer International Publishing; 2015, p. 79–87.

[63] Mendrik A, Vonken EPA, Dankbaar JW, Prokop M, van Ginneken B. Noise filtering in thin-slice 4D cerebral CT perfusion scans. In: Benoit M. Dawant; David R. Haynor, editor. SPIE Med. Imaging Image Process., vol. 7623, San Diego: 2010, p. 76230N1–76230N8. doi:10.1117/12.843813.

[64] Eklund A, Andersson M, Knutsson H. True 4D image denoising on the GPU. Int J Biomed Imaging 2011;2011. doi:10.1155/2011/952819.

[65] Gal Y, Mehnert a J, Bradley a P, McMahon K, Kennedy D, Crozier S. Denoising of dynamic contrast-enhanced MR images using dynamic nonlocal means. IEEE Trans Med Imaging 2010;29:302–10. doi:10.1109/TMI.2009.2026575.

[66] Kosior JC, Kosior RK, Frayne R. Robust dynamic susceptibility contrast MR perfusion using 4D nonlinear noise filters. J Magn Reson Imaging 2007;26:1514–22. doi:10.1002/jmri.21219.

[67] Zitová B, Flusser J. Image registration methods: a survey. Image Vis Comput 2003;21:977–1000. doi:10.1016/S0262-8856(03)00137-9.

[68] Latham S, Varslot T, Sheppard A. Image Registration : Enhancing and Calibrating X-Ray Micro-Ct Imaging. Int. Symp. Soc. Core Anal., Abu Dhabi, UAE: Society of Core Analysts; 2008, p. 1–12.

[69] Fife JL, Rappaz M, Pistone M, Celcer T, Mikuljan G, Stampanoni M. Development of a laser-based heating system for in situ synchrotron-based X-ray tomographic microscopy. J Synchrotron Radiat 2012;19:352–8. doi:10.1107/S0909049512003287.

[70] Chenouard N, Smal I, de Chaumont F, Maška M, Sbalzarini IF, Gong Y, et al. Objective comparison of particle tracking methods. Nat Methods 2014;11:281–9. doi:10.1038/nmeth.2808.

[71] Maška M, Ulman V, Svoboda D, Matula P, Matula P, Ederra C, et al. A benchmark for comparison of cell tracking algorithms. Bioinformatics 2014;30:1609–17. doi:10.1093/bioinformatics/btu080.

[72] Coraluppi S, Carthel C. Multi-stage multiple-hypothesis tracking. ISIF J Adv Inf Fusion 2011;6:57–68.

[73] Chenouard N, Bloch I, Olivo-Marin JC. Multiple hypothesis tracking in microscopy images. Proc - 2009 IEEE Int Symp Biomed Imaging From Nano to Macro, ISBI 2009 2009:1346–9. doi:10.1109/ISBI.2009.5193314.

[74] Mader K. Quantitative big imaging: dynamic experiments 2014. https://rawgithub.com/kmader/Quantitative-Big-Imaging-Course/master/Lectures/09-Dynamic.pdf (accessed February 10, 2015).

[75] Bay BK, Smith TS, Fyhrie DP, Saad M. Digital volume correlation: Three-dimensional strain mapping using X-ray tomography. Exp Mech 1999;39:217–26. doi:10.1007/BF02323555.

[76] Armstrong RT, Berg S. Interfacial velocities and capillary pressure gradients during Haines jumps. Phys Rev E 2013;88:43010. doi:10.1103/PhysRevE.88.043010.

[77] Armstrong RT, Ott H, Georgiadis A, Rücker M, Schwing A, Berg S. Subsecond pore-scale displacement processes and relaxation dynamics in multiphase flow. Water Resour Res 2014:n/a – n/a. doi:10.1002/2014WR015858.

[78] Armstrong RT, Evseev N, Koroteev D, Berg S. Interfacial velocities and the resulting velocity field during a Haines jump. Int. Symp. Soc. Core Anal., Avignon, France: Society of Core Analysts; 2014, p. 1–12.

[79] Dierick M, Van Loo D, Masschaele B, Van den Bulcke J, Van Acker J, Cnudde V, et al. Recent micro-CT scanner developments at UGCT. Nucl Instruments Methods Phys Res Sect B Beam Interact with Mater Atoms 2014;324:35–40. doi:10.1016/j.nimb.2013.10.051.

[80] Avraam DG, Payatakes AC. Flow Mechanisms, Relative Permeabilities, and Coupling Effects in Steady-State Two-Phase Flow through Porous Media. The Case of Strong Wettability. Ind Eng Chem Res 1999;38:778–86. doi:10.1021/ie980404o.

[81] Bultreys T, Boone MA, Boone MN, De Schryver T, Masschaele B, Hoorebeke L Van, et al. Real-time visualization of Haines jumps in sandstone with laboratory-based micro-computed tomography 2015;Submitted.

[82] Rolle M, Hochstetler D, Chiogna G, Kitanidis PK, Grathwohl P. Experimental Investigation and Pore-Scale Modeling Interpretation of Compound-Specific Transverse Dispersion in Porous Media. Transp Porous Media 2012;93:347–62. doi:10.1007/s11242-012-9953-8.

[83] Blunt MJ, Bijeljic B, Dong H, Gharbi O, Iglauer S, Mostaghimi P, et al. Pore-scale imaging and modelling. Adv Water Resour 2013;51:197–216. doi:10.1016/j.advwatres.2012.03.003.

[84] Daccord G, Lenormand R, Liétard O. Chemical dissolution of a porous medium by a reactive fluid-I. Model for the "wormholing" phenomenon. Chem Eng Sci 1993;48:169–78. doi:10.1016/0009-2509(93)80293-Y.

[85] Gharbi O, Bijeljic B, Boek E, Blunt MJ. Changes in Pore Structure and Connectivity Induced by CO2 Injection in Carbonates: A Combined Pore-Scale Approach. Energy Procedia 2013;37:5367–78. doi:10.1016/j.egypro.2013.06.455.

[86] Fourar M, Radilla G. Non-Fickian description of tracer transport through heterogeneous porous media. Transp Porous Media 2009;80:561–79. doi:10.1007/s11242-009-9380-7.

[87] Ott H, Oedai S, Pentland CH, Linden a J Van Der. CO2 Reactive Transport in Limestone : Flow Regimes , Fluid Flow and Mechanical Rock Properties. Int. Symp. Soc. Core Anal., Napa Valley, USA: Society of Core Analysts; 2013, p. 1–12.

[88] Koestel J, Larsbo M. Imaging and quantification of preferential solute transport in soil macropores. Water Resour Res 2014;50:4357–78. doi:10.1002/2014WR015351.

[89] Clausnitzer V, Hopmans JW. Pore-scale measurements of solute breakthrough using microfocus X-ray computed tomography. Water Resour Res 2000;36:2067. doi:10.1029/2000WR900076.

[90] Bijeljic B, Raeini A, Mostaghimi P, Blunt M. Predictions of non-Fickian solute transport in different classes of porous media using direct simulation on pore-scale images. Phys Rev E 2013;87:013011. doi:10.1103/PhysRevE.87.013011.

[91] Ovaysi S, Piri M. Pore-scale modeling of dispersion in disordered porous media. J Contam Hydrol 2011;124:68–81. doi:10.1016/j.jconhyd.2011.02.004.

[92] Bultreys T, Van Hoorebeke L, Cnudde V. Multi-scale, micro-computed tomography-based pore network models to simulate drainage in heterogeneous rocks. Adv Water Resour 2015;78:36–49. doi:10.1016/j.advwatres.2015.02.003.

[93] Mehmani A, Prodanović M. The effect of microporosity on transport properties in porous media. Adv Water Resour 2014;63:104–19. doi:10.1016/j.advwatres.2013.10.009.

[94] Roels S, Elsene J, Carmeliet J, Hens H. Characterisation of pore structure by combining mercury porosimetry and micrography. Mater Struct 2001;34:76–82.